Time-Dependent Ginzburg—Landau Simulations of the Critical Current in Superconducting Films and Junctions in Magnetic Fields

Alexander I. Blair and Damian P. Hampshire

Understanding the magnetic field dependence of the critical current density (J_c) of superconductors is of considerable interest for optimizing their use in high field applications. Using time-dependent Ginzburg—Landau theory, we have completed simulations of the average electric field generated in thin film systems subject to transport currents in applied magnetic fields, and compared them to thin film systems containing narrow junctions of reduced critical temperature (T_c). For thin films in contact with insulating surfaces, J_c approaches the depairing current density at applied magnetic fields below the initial vortex penetration field and remains non-zero until close to the Tinkham's parallel critical field [1]. For thin films in contact with highly metallic surfaces, J_c was found to decrease to zero with decreasing film width. Adding a junction region to the film was found to broaden the transition to the normal state at all applied magnetic fields and reduce J_c of the film at zero field.

***Index Terms*—TDGL, thin films, junctions, critical current density.**

I. Introduction

Understanding how the critical current density J_c of technological superconductors depends on applied magnetic fields is essential to the design and optimization of superconducting devices for applications in high magnetic fields, such as magnet systems for fusion devices. However, accurate simulation of J_c is challenging, since it is highly dependent on interactions between the vortices and the microstructure present in the material. To this end, simulations based on the time-dependent Ginzburg—Landau (TDGL) equations have been widely applied to model vortex dynamics in superconductors, due to their relative simplicity compared to full microscopic theory. Indeed, TDGL simulations have recently also been used to predict optimal pinning landscapes in superconductors containing spherical, spheroidal and columnar pinning centers [2, 3].

The simplest complete set of time-dependent Ginzburg—Landau equations were first derived from microscopic theory for a gapless superconductor dominated by paramagnetic impurities close to its critical temperature by Gor'kov and Eliashberg [4]. The normalized TDGL equations can be written as [5]

$$\eta(\partial_t + \imath\Phi)\psi = [(\boldsymbol{\nabla} - \imath\boldsymbol{A})^2 + \epsilon(\boldsymbol{r}) - |\psi|^2]\psi, \tag{1}$$

$$\kappa^2(\boldsymbol{\nabla} \times \boldsymbol{\nabla} \times \boldsymbol{A}) = \mathrm{Im}[\psi^*(\boldsymbol{\nabla} - \imath\boldsymbol{A})\psi] + (-\boldsymbol{\nabla}\Phi - \partial_t\boldsymbol{A}), \tag{2}$$

with associated boundary conditions

$$(\boldsymbol{\nabla} \times \boldsymbol{A} - \boldsymbol{B}) \times \hat{\boldsymbol{n}} = \boldsymbol{0}, \tag{3}$$

$$(\boldsymbol{\nabla} - \imath\boldsymbol{A})\psi \cdot \hat{\boldsymbol{n}} = -\gamma\psi, \tag{4}$$

where $\hat{\boldsymbol{n}}$ is the outward pointing normal unit vector of the superconductor surface. Distances are normalized in units of the superconductor coherence length ξ, time t in units of $\tau = \mu_0\sigma\kappa^2\xi^2$, the order parameter ψ in units of the bulk Meissner state order parameter ψ_0, the magnetic field in units of the upper critical field B_{c2}, the magnetic vector potential $\boldsymbol{A}$ in units of $B_{c2}\xi$, and the electrostatic potential Φ in units of $B_{c2}\xi^2\tau^{-1}$. $\epsilon(\boldsymbol{r}) = (T - T_c(\boldsymbol{r}))/(T - T_c^S)$ is dependent on the temperature T, the local critical temperature $T_c(\boldsymbol{r})$ and the critical temperature of the bulk superconductor T_c^S. Current densities are scaled in units of the depairing current density of the superconductive domain $J_D = 2B_{c2}/3\sqrt{3}\mu_0\xi\kappa^2$. Eqs. (1) – (4) along with Maxwell's equations define the state of the system up to a gauge transformation [6].

The dimensionless parameters κ and η characterize the superconductive material. κ is the well-known Ginzburg—Landau parameter that represents the ratio of the characteristic length scales for variations in the electromagnetic field and variations in the order parameter. Similarly, the friction coefficient η represents the ratio between the characteristic timescales for the evolution of the electromagnetic field and evolution of the order parameter field. In terms of the normal state conductivity σ and the diffusivity D, the friction coefficient $\eta = (\mu_0\sigma D\kappa^2)^{-1}$, which was shown by Schmid to have the limiting value of $\eta = 5.78$ in the dirty limit [7]. The surface parameter γ is the reciprocal of the De Gennes extrapolation

This work is funded by EPSRC grant EP/L01663X/1 for the Fusion Doctoral Training Network. This work has been carried out within the framework of the EUROfusion Consortium and has received funding from the Euratom research and training programme 2014-2018 under grant agreement No 633053. Data are available at: http://dx.doi.org/10.15128/r15d86p0202 and associated materials are on the Durham Research Online website: http://dro.dur.ac.uk/.

A. I. Blair and D. P. Hampshire are with Durham University, Department of Physics, Superconductivity Group, South Road, Durham, DH1 3LE, UK (e-mail: a.i.blair@durham.ac.uk).

Color versions of one or more of the figures in this paper are available online at http://ieeexplore.ieee.org.

Digital Object Identifier will be inserted here upon acceptance.

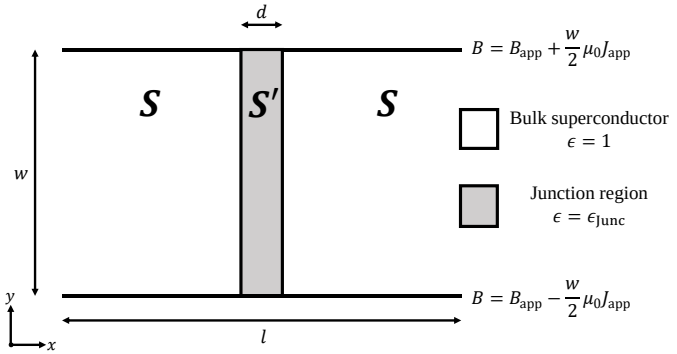

Fig. 1. Schematic diagram of the simulated thin film system, periodic in the x direction, containing a junction region of thickness d. Magnetic fields are applied along the *z*-direction. For the thin film case, $d = 0$ and $\epsilon = 1$ throughout.

length (in normalized units) and has limiting values of $\gamma = 0$ for surfaces in contact with an insulator (or vacuum) and $\gamma = \infty$ for highly metallic surfaces [8].

Numerical solutions to the TDGL equations have been previously used by Machida to generate simulated *V-I* characteristics for a small superconducting system [9]. This was extended by Berdiyorov et al. to generate *V-I* characteristics and model vortex dynamics in superconducting stripes and periodic junction arrays [10, 11]. Barba-Ortega has investigated the vortex structure in mesoscopic thin films and the effect of modifying surface boundary conditions for such structures on their magnetization [12, 13]. TDGL theory has also been used to investigate the effect of normal metal coatings on the magnetization characteristics of type-II superconductors [14], and to simulate model polycrystalline systems in 3D [15]. More recently, a stable, large-scale solver of the TDGL equations developed by Sadovskyy et al. [5] has been developed to optimize pinning and J_c in high-temperature superconductive materials [16, 17].

II. Computational Method

In this work, the TDGL equations in the zero electric potential gauge were solved in 2D using the finite difference semi-implicit Crank—Nicolson algorithm developed by Winiecki and Adams [18]. It is based on the widely-used *U–ψ* method described by Gropp et al. [19]. All computations were performed on the Hamilton 7 supercomputing cluster at Durham University.

Thin superconductive films were discretized on a grid with length l, width w and grid spacing 0.4ξ in the *x* and *y*-directions. A time step of $\delta t = 0.5\tau$ was chosen for these simulations, with the observables of the local current density, local supercurrent density and local superelectron density converged to one part in 10^5 at each time step. For computational efficiency, we have taken $\kappa = 10$ and $\eta = 1$ for this system.

Periodic boundary conditions were implemented for the film in the *x*-direction. In the *y*-direction, the ghost point method was used to implement second-order accurate formulations of Eqs. (3) and (4). The magnetic field at the upper and lower surfaces of the film was set by the externally applied field B_{app} and the applied average current density J_{app} according to [9]

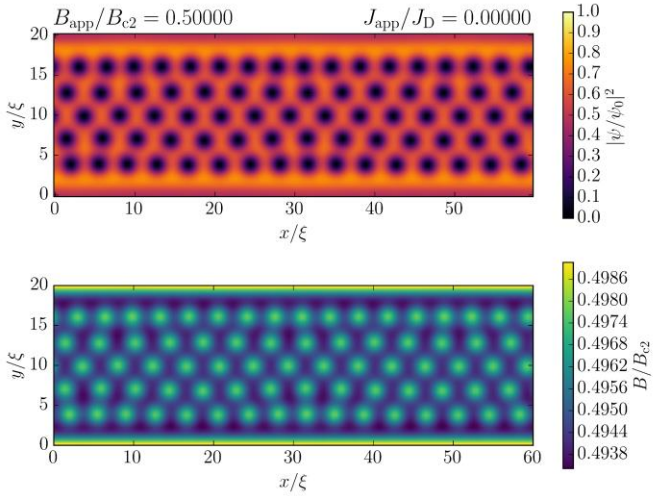

Fig. 2. Normalized superelectron density $|\psi|^2$ (top) and local magnetic field B (bottom) in a superconducting film with $w = 20\xi$, $l = 60\xi$, $\eta = 1$ and $\kappa = 10$ in an applied external magnetic field $B_{app} = 0.5B_{c2}$, equilibrated for $10^4\tau$. The system is periodic in the *x*-direction and insulating boundary conditions were applied in the *y*-direction.

$$B\left(y = \frac{w}{2} \pm \frac{w}{2}\right) = B_{app} \pm \frac{w}{2}\mu_0 J_{app}. \quad (5)$$

Simulations of superconducting thin films in magnetic fields were initialized in the bulk Meissner state throughout ($\psi = 1$, $\boldsymbol{B} = \boldsymbol{J} = \boldsymbol{0}$). The magnetic field at the film surfaces were then raised to the desired applied field B_{app} at a rate of $3 \times 10^{-4}\, B_{c2}\tau^{-1}$ and then held for 3000τ to equilibrate, unless otherwise specified. For thin films containing junctions, a junction region with thickness $d = 2\xi$ was added to the centre of the thin film system, perpendicular to the direction of applied current flow, in which $\epsilon(\boldsymbol{r}) = \epsilon_{Junc}$ inside the junction region; a schematic of this system is shown in Fig. 1. When T_c inside the junction region is reduced relative to the surrounding superconductor, ϵ_{Junc} decreases. An example of the superconducting state for the thin film system at $B_{app} = 0.5\, B_{c2}$ is shown in Fig. 2, with a triangular vortex lattice seen in the bulk of the film.

For simulations of the $E(J)$ characteristics of thin film systems, the applied average transport current density J_{app} was increased at a constant rate of $3 \times 10^{-4}\, J_D\tau^{-1}$ and the average electric field along the *x*-direction $\langle E_x \rangle$ in the system was computed at each time step.

III. Results

A. Thin Films

$E(J)$ characteristics of the thin film system subject to insulating boundary conditions at the upper and lower surfaces are shown in Fig. 3. For low currents, almost dissipationless behavior is observed. For intermediate currents at low applied magnetic fields, temporal oscillations in the average electric field in the film are observed due to the entry/exit of entire rows of vortices across the upper/lower surface barriers of the film. The vortex rows travel across the film with a current-dependent velocity, and thus these electric field oscillations have a corresponding current-dependent period. At higher fields, the defect

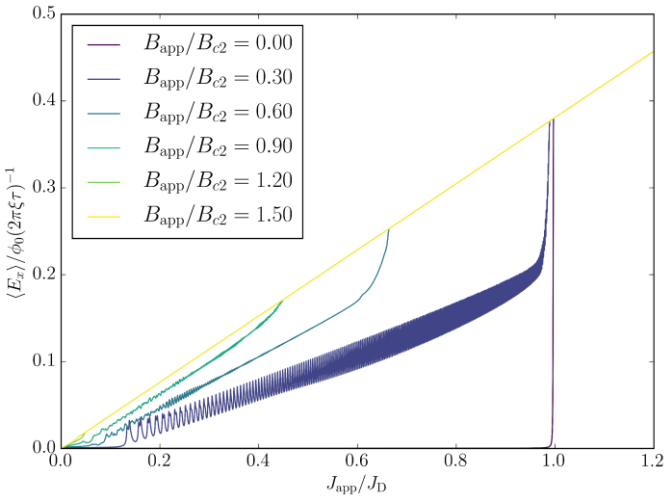

Fig. 3. Average electric field $\langle E_x \rangle$ against external applied current J_{app} for a superconducting film with $w = 20\xi$, $l = 60\xi$, $\eta = 1$ and $\kappa = 10$ subject to various external magnetic fields. Periodic boundary conditions were applied in the *x*-direction and insulating boundary conditions were applied in the *y*-direction. Systems were first initialised in the bulk Meissner state and the external magnetic field B_{app} was raised to the desired value. The external current density J_{app} was then slowly swept up to above the depairing current J_D.

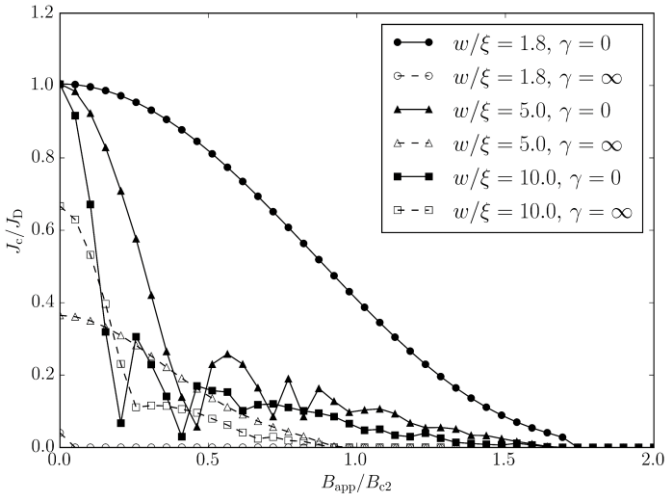

Fig. 4. Critical current density J_c against mean external magnetic field B_{app} for a superconducting system with $\kappa = 10$, $\eta = 1$ and $l = 60\xi$ for varying width w. J_c and B_{app} are expressed in units of the depairing current J_D and the upper critical field B_{c2} for each superconductor respectively. The critical current was determined using Ekin's offset method using a critical electric field $E_c = 0.01\phi_0/2\pi\xi\tau$ and extrapolating to $\langle E_x \rangle = 0$.

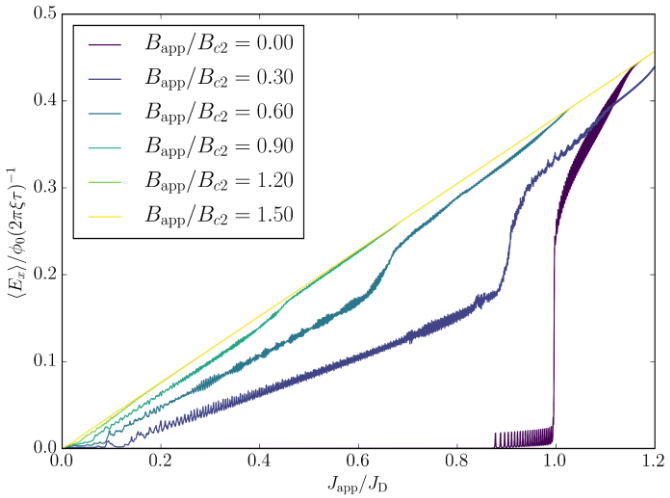

Fig. 5. Average electric field $\langle E_x \rangle$ against external applied current J_{app} for a superconducting film containing a 2ξ wide 'junction' region in its centre, in which the local T_c term $\epsilon_{Junc} = 0.80$. The surrounding superconducting domain was parameterised with $\eta = 1$, $\kappa = 10$ and dimensions $w = 20\xi$ and $l = 60\xi$, with periodic boundary conditions applied in the *x*-direction and insulating boundary conditions applied in the *y*-direction. At each external magnetic field, the system was first initialised in the bulk Meissner state and the external magnetic field B_{app} was raised to the desired value. The external current density J_{app} was then slowly swept up to above the depairing current J_D.

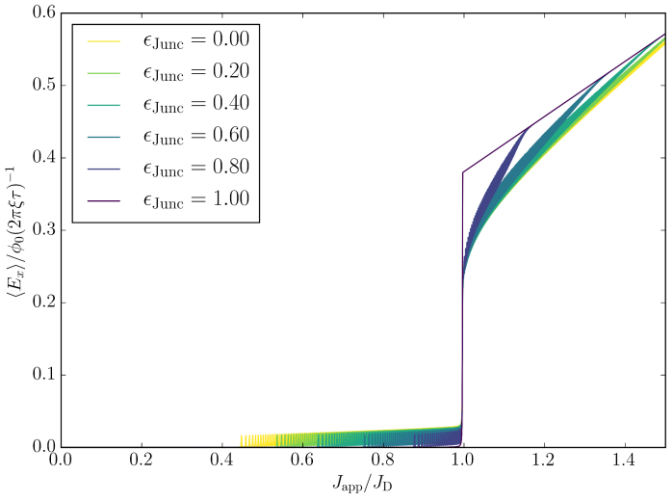

Fig. 6. Average electric field $\langle E_x \rangle$ against external applied current J_{app} for a superconducting film containing a 2ξ wide 'junction' region in its centre, in which the local T_c term ϵ_{Junc} is variable. The surrounding superconducting domain was parameterised with $\eta = 1$, $\kappa = 10$ and dimensions $w = 20\xi$ and $l = 60\xi$, with periodic boundary conditions applied in the *x*-direction and insulating boundary conditions applied in the *y*-direction. At each external magnetic field, the system was first initialised in the bulk Meissner state and the external magnetic field B_{app} was raised to the desired value. The external current density J_{app} was then slowly swept up to above the depairing current J_D.

density in the vortex lattice increases and these electric field oscillations become less clearly defined, as defect motion and the entry/exit of individual vortices dominates over the coherent motion of vortex rows. Eventually, as the applied average current density in the film is increased further, the superconducting film transitions into the (resistive) normal state. This transition becomes more abrupt as the applied magnetic field is increased.

From the $E(J)$ characteristics obtained for the film at various applied magnetic fields, the critical current density J_c was determined using Ekin's offset criterion method [20]. At a critical average electric field $E_c = 0.01\ \phi_0/2\pi\xi\tau$, the local tangent to the $E(J)$ characteristic was found and extrapolated to zero electric field; J_c was taken to be the corresponding current density at this point.

Fig. 4 displays the critical current density as a function of applied magnetic field for superconducting films of varying widths of the superconductor, subject to both highly metallic and insulating surface conditions. At applied magnetic fields much lower than the initial vortex penetration field of the film, the critical current density of films with insulating surface conditions is large, and close to the depairing current density J_D. For films with highly metallic boundary conditions, the critical

current density in this regime tends to zero as the film width decreases, as a result of the suppression of superelectron density close to the highly metallic surfaces.

In low magnetic fields, of the order of the initial vortex penetration field in the film, the critical current density of wide films exhibits a (distorted) Fraunhöfer-like dependence with applied magnetic field. For these films, the critical current density of the film decreases to zero as the applied field is raised above B_{c2} for films subject to highly metallic surface conditions, or above $B_{c3} = 1.69B_{c2}$ for films subject to insulating surface conditions. The critical current density can remain non-zero up to extremely high applied magnetic fields in very thin films with insulating surfaces, depending on their width. High resolution simulations with a grid spacing of 0.1ξ suggest that the field at which the critical current density does vanish for thin films is close to the parallel critical field of the film $B_{c||} = 2\sqrt{3}B_{c2}\xi/w$, consistent with Tinkham's predictions [1].

B. Thin Films Containing Junctions

Next, the effect of including a junction region in the thin film was investigated. Fig. 5 shows that the $E(J)$ characteristics of the thin film system are modified when a junction with $\epsilon_{\mathrm{Junc}} = 0.8$ is added to the film. At large applied current densities, in zero magnetic fields electric field oscillations are introduced, as a result of vortex-antivortex motion along the junction. Furthermore, in all magnetic fields, the transition to the normal state at high current densities is broadened. This occurs because a non-zero superelectron density persists just outside the junction region that carries an associated supercurrent, although most of the superconducting film itself is in the normal state.

Finally, the effects of varying the junction properties on the zero field $E(J)$ characteristic of the film containing a junction are displayed in Fig. 6. When ϵ_{Junc} is reduced, the critical current density decreases and in the high E-field regime, the transition to the normal state broadens and the current density required to drive the whole system into the normal state increases. This behavior has previously been observed by Berdiyorov et al. for the specific case of $\epsilon_{\mathrm{Junc}} = -1$ [11]; our results in Fig. 6 show that this broadening is strongly dependent on the junction T_c.

IV. Discussion

A. Thin Films

The equilibrated vortex state obtained for the thin film at each applied field, prior to applying current flow, is sensitive to noise and the rate of increase of the applied magnetic field. This is because variations in the locations of initial vortex penetration can introduce defects in the vortex lattice. These defects then introduce additional noise in the simulated $E(J)$ characteristics of the film at low applied currents, but provided they are sufficiently few in number, they do not significantly affect the determination of the critical current density of the system provided the offset criterion E_c is large enough. The convergence criteria and field ramp rate used here were selected as to be small and slow enough respectively to minimize the number of defects in the vortex state, whilst remaining large enough to allow the simulations to complete in reasonable timescales.

In simulations of systems in high magnetic fields, because vortex density is higher, the number of defects increases and the resultant $E(J)$ characteristics are unavoidably noisier. This crossover to a defect-dominated lattice at high fields has been previously observed in simulations and experiments carried out by Papari et al. [21]. This affects our results in two ways; firstly, high field states take longer to equilibrate, and secondly, relaxation of the vortex lattice under small applied currents can generate significant transient electric fields as the vortex lattice relaxes from an initial metastable state (c.f. Fig. 3).

B. Thin Films Containing Junctions

Due to the presence of the junction region in these simulations, the vortex lattice is more disordered than for the thin film alone and equilibration of the vortex lattice takes longer. The noise in the resultant $E(J)$ characteristics in magnetic fields is greater as a result. Longer equilibration times are required to avoid this, but are more computationally demanding. This has limited our ability to obtain $J_c(B)$ data for the junction system. Furthermore, the junction region modelled in this work is highly simplified as just a region of reduced T_c, without considering any variations of κ or η inside the junction. These issues will be the subject of future studies.

V. Conclusion

We have performed TDGL simulations to describe the evolution of the vortex lattice in thin films subject to transport current in a magnetic field, with and without the inclusion of narrow junctions of reduced T_c. We have found that the critical current density of thin films with insulating surface conditions approaches the depairing current density at applied magnetic fields below the initial vortex penetration field. In contrast, the critical current density of thin films with highly metallic surface conditions decreases to zero as the film width decreases, due to the suppression of the local superelectron density close to the metallic surfaces. Furthermore, we have found that the critical current density in very thin films with insulating surfaces subject to applied magnetic fields is limited by the parallel critical field $B_{c||} = 2\sqrt{3}B_{c2}\xi/w$, consistent with Tinkham's analytic results. Finally, when narrow junction regions of reduced T_c are added to the thin film perpendicular to the direction of current flow, we observe a suppression of the critical current of the system in zero applied magnetic field and a broadening of the transition to the normal state at all applied magnetic fields.

Acknowledgment

The authors would like to thank P. Branch and L. Heck for useful discussions. This work made use of the facilities of the Hamilton HPC Service of Durham University.

REFERENCES

[1] M. Tinkham, *Introduction to Superconductivity*, 2nd ed. Singapore: McGraw-Hill Book Co., 1996, pp. 110-147.

[2] A. E. Koshelev, I. A. Sadovskyy, C. L. Phillips, and A. Glatz, "Optimization of vortex pinning by nanoparticles using simulations of the time-dependent Ginzburg-Landau model," *Physical Review B*, vol. 93, no. 6, p. 060508, 02/29/ 2016.

[3] G. Kimmel, I. A. Sadovskyy, and A. Glatz, "In silico optimization of critical currents in superconductors," *Physical Review E*, vol. 96, no. 1, p. 013318, 07/27/ 2017.

[4] L. P. Gor'kov and G. M. Eliashberg, "Generalization of the Ginzburg-Landau equations for non-stationary problems in the case of alloys with paramagnetic impurities," *Soviet Physics JETP*, vol. 27, no. 2, pp. 328-334, 1968.

[5] I. A. Sadovskyy, A. E. Koshelev, C. L. Phillips, D. A. Karpeyev, and A. Glatz, "Stable large-scale solver for Ginzburg–Landau equations for superconductors," *Journal of Computational Physics*, vol. 294, pp. 639-654, 8/1/ 2015.

[6] J. Fleckinger-Pelle and H. G. Kaper, *Gauges for the Ginzburg-Landau equations of superconductivity* (Conference: International congress on industrial and applied mathematics, Hamburg (Germany), 3-7 Jul 1995; Other Information: PBD: [1995]). ; Argonne National Lab., IL (United States), 1995, p. Medium: ED; Size: 4 p.

[7] A. Schmid, "A Time dependent Ginzburg-Landau Equation and its Application to the problem of resistivity in the Mixed State," *Physik der Kondensierte Materie*, vol. 5, pp. 302-317, 1966.

[8] P. G. De Gennes, *Superconductivity of Metals and Alloys*. Boulder, Colorado: Perseus Books Group, 1999.

[9] M. Machida and H. Kaburaki, "Direct simulation of the time-dependant Ginzburg-Landau equation for Type-II superconducting thin film: Vortex dynamics and V-I characteristics," *Physical Review Letters*, vol. 71, no. 19, pp. 3206-3209, 1993.

[10] G. R. Berdiyorov, M. V. Milošević, and F. M. Peeters, "Kinematic vortex-antivortex lines in strongly driven superconducting stripes," *Physical Review B*, vol. 79, no. 18, p. 184506, 05/06/ 2009.

[11] G. R. Berdiyorov, A. R. de C. Romaguera, M. V. Milošević, M. M. Doria, L. Covaci, and F. M. Peeters, "Dynamic and static phases of vortices under an applied drive in a superconducting stripe with an array of weak links," *The European Physical Journal B*, journal article vol. 85, no. 4, p. 130, April 24 2012.

[12] J. J. Barba, C. C. de Souza Silva, L. R. E. Cabral, and J. Albino Aguiar, "Flux trapping and paramagnetic effects in superconducting thin films: The role of de Gennes boundary conditions," *Physica C: Superconductivity and its Applications*, vol. 468, no. 7, pp. 718-721, 2008/04/01/ 2008.

[13] J. Barba-Ortega, A. Becerra, and J. Albino Aguiar, "Two dimensional vortex structures in a superconductor slab at low temperatures," *Physica C: Superconductivity*, vol. 470, no. 3, pp. 225-230, 2010/02/01/ 2010.

[14] G. J. Carty, M. Machida, and D. P. Hampshire, "Numerical studies on the effect of normal metal coatings on the magnetisation characteristics of type-II superconductors," *Physical Review B*, vol. 71, p. 144507, 2005.

[15] G. J. Carty and D. P. Hampshire, "Visualising the mechanism that determines the critical current density in polycrystalline superconductors using time-dependent Ginzburg-Landau theory," *Physical Review B*, vol. 77, p. 172501, 2008.

[16] I. A. Sadovskyy *et al.*, "Toward Superconducting Critical Current by Design," *Advanced Materials*, vol. 28, no. 23, pp. 4593-4600, 2016.

[17] I. A. Sadovskyy, A. E. Koshelev, A. Glatz, V. Ortalan, M. W. Rupich, and M. Leroux, "Simulation of the Vortex Dynamics in a Real Pinning Landscape of $YBa_2Cu_3O_{7-\delta}$ Coated Conductors," *Physical Review Applied*, vol. 5, no. 1, p. 014011, 01/27/ 2016.

[18] T. Winiecki and C. S. Adams, "A Fast Semi-Implicit Finite Difference Method for the TDGL Equations," *Journal of Computational Physics*, vol. 179, pp. 127-139, 2002.

[19] W. D. Gropp, H. G. Kaper, G. K. Leaf, D. M. Levine, M. Palumbo, and V. M. Vinokur, "Numerical simulation of vortex dynamics in Type-II superconductors," *Journal Comput Phys*, vol. 123, pp. 254-266, 1996.

[20] J. W. Ekin, *Experimental Techniques for Low-Temperature Measurements*. New York: Oxford University Press, 2007.

[21] G. P. Papari *et al.*, "Geometrical vortex lattice pinning and melting in YBaCuO submicron bridges," *Scientific Reports*, Article vol. 6, p. 38677, 12/23/online 2016.